

Thermal conductance and thermoelectric figure of merit of C₆₀-based single-molecule junctions: electrons, phonons, and photons

J. C. Klöckner^{1,*}, R. Siebler¹, J. C. Cuevas², and F. Pauly¹

¹*Department of Physics, University of Konstanz, D-78457 Konstanz, Germany and*

²*Departamento de Física Teórica de la Materia Condensada and Condensed Matter Physics Center (IFIMAC), Universidad Autónoma de Madrid, E-28049 Madrid, Spain*

(Dated: March 5, 2022)

Motivated by recent experiments, we present here an *ab initio* study of the impact of the phonon transport on the thermal conductance and thermoelectric figure of merit of C₆₀-based single-molecule junctions. To be precise, we combine density functional theory with nonequilibrium Green's function techniques to compute these two quantities in junctions with either a C₆₀ monomer or a C₆₀ dimer connected to gold electrodes, taking into account the contributions of both electrons and phonons. Our results show that for C₆₀ monomer junctions phonon transport plays a minor role in the thermal conductance and, in turn, in the figure of merit, which can reach values on the order of 0.1, depending on the contact geometry. In C₆₀ dimer junctions, phonons are transported less efficiently, but they completely dominate the thermal conductance and reduce the figure of merit as compared to monomer junctions. Thus, claims that by stacking C₆₀ molecules one could achieve high thermoelectric performance, which have been made without considering the phonon contribution, are not justified. Moreover, we analyze the relevance of near-field thermal radiation for the figure of merit of these junctions within the framework of fluctuational electrodynamics. We conclude that photon tunneling can be another detrimental factor for the thermoelectric performance, which has been overlooked so far in the field of molecular electronics. Our study illustrates the crucial roles that phonon transport and photon tunneling can play, when critically assessing the performance of molecular junctions as potential nanoscale thermoelectric devices.

I. INTRODUCTION

Molecular junctions have turned out to be ideal systems to explore and establish the fundamental principles that govern charge and energy transport at the nanoscale [1, 2]. In particular, recent experimental advances have made possible to study key aspects of energy and heat conduction in molecular junctions such as thermoelectricity [3], Joule heating [4], and thermal conductance [5]. In this sense, the investigation of phonon transport in these atomic-scale junctions is presently attracting a lot of attention for two basic reasons. On the one hand, molecular junctions offer the possibility to study phonon conduction in an interesting regime, where the system size is smaller than the phonon inelastic mean free path. On the other hand, the phonon contribution to the thermal conductance plays a fundamental role, when assessing the performance of molecular junctions as thermoelectric devices. This performance is characterized by the so-called figure of merit ZT , which is given by a combination of several transport quantities as follows [6]

$$ZT = \frac{GS^2T}{\kappa} = \frac{Z_{\text{el}}T}{1 + \kappa_{\text{other}}/\kappa_{\text{el}}}. \quad (1)$$

Here, G is the electrical conductance, S the thermopower, T the absolute temperature, and κ the thermal conductance. Strictly speaking, this thermal conductance should include all possible contributions, and it can be

written as $\kappa = \kappa_{\text{el}} + \kappa_{\text{other}}$, where κ_{el} is the electronic contribution and κ_{other} includes the contributions of other heat carriers like that of phonons and photons. By bringing Eq. (1) into the form on the right hand side using $Z_{\text{el}}T = GS^2T/\kappa_{\text{el}}$, it is obvious that any additional heat transport contribution (beyond electrons) will be detrimental for the thermoelectric performance, since ZT needs to be maximized. Therefore, the experimental and theoretical determination of κ_{other} is crucial to critically evaluate, whether molecular junctions can potentially operate as efficient nanoscale thermoelectric devices.

The most obvious additional contribution to the heat conductance in molecular junctions is that of phonons, a topic that is currently attracting a lot of attention. For a recent review, we recommend Ref. 5. However, photons can also give a significant contribution to the total heat conductance. Molecular junctions actually constitute nanoscale gaps between metal surfaces, bridged by few or single molecules. Thus, even if the experiments are carried out in ultra-high vacuum conditions, one should also consider the contribution of thermal radiation or photon tunneling. It has been understood that when two bodies are brought sufficiently close together (with a separation below the thermal wavelength, which is 9.6 μm at room temperature), near-field contributions in the form of evanescent waves dominate the radiative heat transfer and lead to a huge enhancement of the radiative thermal conductance [7]. This near-field radiative heat transfer (NFRHT) can exceed by orders of magnitude the limit set by the Stefan-Boltzmann law for black bodies, see Ref. 8 for a recent review. These ideas have been experimentally verified in recent years, and advances in nanothermome-

* Corresponding author: Jan.Kloekner@uni-konstanz.de

try have even made possible to explore thermal radiation in the extreme near-field regime, where objects are separated by gaps of a few nanometers and even below [9–13]. This aspect of photonic heat conduction has traditionally been ignored thus far in the field of molecular electronics.

The main goal of this work is to rigorously compute the contribution κ_{pn} of phonons to both the thermal conductance and the figure of merit in C_{60} -based single-molecule junctions using parameter-free *ab initio* electronic structure methods. But also the photonic part κ_{pt} will be estimated using simple models for the molecular junction geometries within the framework of fluctuational electrodynamics. We will thus ultimately consider $\kappa = \kappa_{\text{el}} + \kappa_{\text{pn}} + \kappa_{\text{pt}}$ in the following, i.e., a thermal conductance κ consisting of electronic (el), phononic (pn), and photonic (pt) parts.

The fullerene C_{60} is a test-bed molecule for molecular electronics and its electrical transport properties have been extensively investigated both experimentally [14–22] and theoretically [18, 20–32]. Also in the context of thermoelectricity, C_{60} -based single-molecule junctions have been analyzed and several groups have reported room-temperature thermopower measurements [33–35]. In particular, Evangeli *et al.* [34] employed a scanning tunneling microscope (STM) setup to report simultaneous measurements of the conductance and thermopower in “single- C_{60} ” or monomer molecular junctions with Au electrodes. They showed that these junctions can exhibit thermopower values ranging from -40 to 0 $\mu\text{V}/\text{K}$, depending of the contact details, with a mean value of -18 $\mu\text{V}/\text{K}$. The findings agree well with theoretical expectations that predict that these negative values are due to charge transport that is dominated by the lowest unoccupied molecular orbital (LUMO) [31]. Moreover, these authors were able to pick up C_{60} molecules with the STM tip and subsequently use them to contact another individual C_{60} molecule, forming in this way molecular junctions with a C_{60} dimer bridging the gap between the Au electrodes. These “two- C_{60} ” or dimer molecular junctions were shown to exhibit negative thermopower values of up to -72 $\mu\text{V}/\text{K}$ with an average value of -33 $\mu\text{V}/\text{K}$. This almost doubles the magnitude observed in the monomer junctions, as it is generally expected for increasing molecular length in the off-resonant transport regime [36]. These results, together with first-principles transport calculations, led the authors to suggest that stacks of C_{60} molecules could provide a way to achieve high ZT values (even above 1), making fullerene-based junctions very promising for thermoelectric applications. However, it is worth stressing that this appealing suggestion was made without taking into account the phonon contribution in the *ab initio* calculations and without measuring the thermal conductance. Indeed experimental setups were until recently not sensitive enough to measure κ at the atomic scale, and single-molecule junctions have yet to be examined with newly developed tools [37]. Thus, this interesting suggestion still has to stand careful theoretical and experimental tests with access to all the

major quantities determining the figure of merit.

The goal of this work is to fill this gap from the theoretical point of view. For this purpose, we present here a detailed study of the role of the phonon transport in both the thermal conductance and the figure of merit of monomer and dimer C_{60} molecular junctions. This study is based on a state-of-the-art combination of density functional theory (DFT) with nonequilibrium Green’s function (NEGF) techniques [38, 39], which allows us to compute the contribution of both electrons and phonons to the different transport properties. Our results show that the phonons play a minor role in the thermal conductance of the monomer junctions, while they largely determine this property in dimer junctions. This fact results in a substantial reduction of the ZT values of the dimer junctions, as compared to the monomer junctions, in spite of the fact that phonons are transported less efficiently in the dimer case. In other words, our results do not back up the suggestion above, but instead they show that phonons severely limit the thermoelectric performance of dimer junctions. In addition, we provide in this work a critical analysis of the impact of thermal radiation on the ZT values of molecular junctions, a factor that has been overlooked so far in molecular electronics. We show, in particular, that the NFRHT between the metallic electrodes can indeed further reduce the figure of merit of molecular junctions. This effect is particularly pronounced in the tunneling regime. Overall, our work demonstrates the importance of taking into account both phonons and photons for a proper evaluation of the performance of molecular junctions as possible thermoelectric devices. Moreover, it provides valuable insights into the relative contribution of different heat carriers to the thermal conductance, namely electrons, phonons, and photons.

The rest of the paper is organized as follows. First, in section II we briefly describe the theoretical methods employed to obtain the results presented in this work. Then, in section III we discuss the main results, concerning in subsection III A the impact of phonons on the thermal conductance and figure of merit of C_{60} -based molecular junctions and in subsection III B the importance of near-field thermal radiation. Finally, we summarize in section IV our main conclusions.

II. THEORETICAL APPROACH

Our primary goal is to compute the different charge and energy transport properties that determine the figure of merit of single-molecule junctions. Electronic and phononic ones are treated within the framework of the Landauer-Büttiker approach to coherent transport. For this purpose, we make use of the first-principles formalism developed by us and reported in Refs. 38–40. Our approach is based on a combination of DFT and NEGF techniques and allows us to compute all of the basic thermoelectric linear response transport properties of a

nanoscale system, namely G , S , κ_{el} and κ_{pn} . Photon transport, on the other hand, is described within the framework of fluctuational electrodynamics. In particular, we compute κ_{pt} for nanometer-sized gaps following Ref. 41. In what follows, we briefly describe the main features of our methods and refer to the above-mentioned references for further details.

A. Contact geometries, electronic structure, and vibrational properties

Our modeling starts with the construction of the molecular junction geometries. We use DFT to obtain equilibrium geometries through total energy minimization and to compute their electronic structure. Vibrational properties of the optimized equilibrium contacts are subsequently obtained in the framework of density functional perturbation theory. For these purposes, we use procedures as implemented in the quantum chemistry software package TURBOMOLE 6.5 [42–44]. In our DFT calculations we employ the Perdew-Burke-Ernzerhof exchange-correlation functional [45, 46] with the Grimme dispersion correction [47], the default2 basis set of split-valence-plus-polarization quality def2-SV(P) [48], and the corresponding Coulomb fitting basis [49]. In order to accurately determine the vibrational energies and force constants, we use very strict convergence criteria. In particular, total energies are converged to a precision of better than 10^{-9} a.u., whereas geometry optimizations are performed until the change of the maximum norm of the Cartesian gradient is below 10^{-5} a.u..

B. Electronic transport

Within the Landauer-Büttiker picture, the contribution of electrons to the different transport properties is determined by the energy-dependent electronic transmission $\tau_{\text{el}}(E)$. In particular, in the linear response regime, in which we are interested in, the electrical conductance G , thermopower S , and the electronic thermal conductance κ_{el} are given by [1, 50]

$$G = G_0 K_0, \quad (2)$$

$$S = -\frac{K_1}{eTK_0}, \quad (3)$$

$$\kappa_{\text{el}} = \frac{2}{hT} \left(K_2 - \frac{K_1^2}{K_0} \right), \quad (4)$$

where $e = |e|$ is the absolute value of the electron charge, h is Planck's constant, k_B is Boltzmann's constant, T is the average junction temperature, and $G_0 = 2e^2/h$ is the conductance quantum. The coefficients K_n in Eqs. (2)–(4) are given by

$$K_n = \int_{-\infty}^{\infty} dE \tau_{\text{el}}(E) \left(-\frac{\partial f(E)}{\partial E} \right) (E - \mu)^n, \quad (5)$$

where $f(E) = \{\exp[(E - \mu)/k_B T] + 1\}^{-1}$ is the Fermi function. Here, the chemical potential $\mu \approx E_F$ is approximately given by the Fermi energy E_F of the Au electrodes. Dependences of transport quantities, the coefficients K_n and the Fermi function on temperature and chemical potential have been suppressed.

Let us emphasize that we have used the exact Eqs. (2)–(4) in our calculations, but it is instructive to have in mind the corresponding low-temperature expansions, which turn out to be very good approximations in almost all cases. They read

$$G \approx G_0 \tau_{\text{el}}(E_F), \quad (6)$$

$$S \approx -\frac{\pi^2 k_B^2 T}{3e} \left. \frac{\partial_E \tau_{\text{el}}(E)}{\tau_{\text{el}}(E)} \right|_{E=E_F}, \quad (7)$$

$$\kappa_{\text{el}} \approx L_0 G T. \quad (8)$$

The latter expression for κ_{el} is known as the Wiedemann-Franz law [1] and $L_0 = (k_B/e)^2 \pi^2/3$ is the Lorentz number.

We have computed the electron transmission by making use of our DFT-NEGF formalism, implemented in TURBOMOLE and explained in detail in Ref. 40. In particular, to construct the electrode surface Green's function, we use a broadening of $\eta = 10^{-2}$ a.u. and 32×32 k -points in the transverse direction, which was found to be sufficient to converge the electronic transport coefficients.

C. Phonon transport

In analogy with the electronic part, we have computed the phononic contribution to the heat conductance within the framework of the Landauer-Büttiker picture. By choosing this procedure, we ignore anharmonic effects that are expected to play a minor role in short molecular junctions like the ones studied here [5]. Within this picture, the phonon contribution to the heat conductance in the linear regime can be expressed in terms of the phononic transmission function $\tau_{\text{pn}}(E)$ as follows [51, 52]

$$\kappa_{\text{pn}} = \frac{1}{h} \int_0^\infty dE E \tau_{\text{pn}}(E) \frac{\partial n(E, T)}{\partial T}, \quad (9)$$

where $n(E, T) = [\exp(E/k_B T) - 1]^{-1}$ is the Bose function. As for the electronic transport quantities, we have suppressed the temperature dependence of κ_{pn} .

For computing the phononic thermal conductance, we need to determine the energy-dependent phonon transmission $\tau_{\text{pn}}(E)$. To do so, we have employed the procedures described in Refs. 38 and 39. A broadening of $\eta = 10^{-5}$ a.u. and 32×32 k -points in the transverse direction were used to obtain well-converged phononic transport properties.

D. Photon transport

We use fluctuational electrodynamics [53] to determine κ_{pt} . This formulation of NFRHT was indeed employed recently to study the radiative heat transfer between a gold surface and a gold tip in the extreme near-field regime and shown to work nicely all the way down to gaps of a few nanometers [11].

Our calculation of the radiative thermal conductance κ_{pt} proceeds in two steps. First, we calculate the so-called heat transfer coefficient, i.e. the linear radiative thermal conductance per unit area, for two Au infinite parallel plates, and then we use this result together with the so-called proximity approximation (see below) to compute κ_{pt} for two different geometries (see Fig. 9(a)): (i) a tip-surface geometry and (ii) a tip-tip geometry.

Within the framework of fluctuational electrodynamics [53] the heat transfer coefficient ζ for two infinite parallel plates separated by a distance Δ is given by [7]

$$\zeta(\Delta) = \int_0^\infty \frac{d\omega}{2\pi} \frac{\partial \Theta(\omega, T)}{\partial T} \int \frac{d^2 k_{\parallel}}{(2\pi)^2} \tau_{\text{pt}}(\omega, \mathbf{k}_{\parallel}), \quad (10)$$

where $\Theta(\omega, T) = \hbar\omega n(E, T)$, ω is the radiation frequency, $\mathbf{k} = (k_{\perp}, \mathbf{k}_{\parallel})$ is the wavevector expressed in terms of components perpendicular and parallel to the surface planes with $k_{\perp} = k_x$ and $\mathbf{k}_{\parallel} = (k_y, k_z)$, $\tau_{\text{pt}}(\omega, \mathbf{k}_{\parallel})$ is the total transmission probability of the electromagnetic waves, and we have omitted the temperature dependence of ζ . Notice that the second integral in Eq. (10) is carried out over all possible directions of \mathbf{k}_{\parallel} , and it includes the contribution of both propagating waves with $k_{\parallel} < \omega/c$ and evanescent waves with $k_{\parallel} > \omega/c$, where $k_{\parallel} = |\mathbf{k}_{\parallel}|$ and c is the velocity of light in vacuum. The total transmission can be written as $\tau_{\text{pt}}(\omega, \mathbf{k}_{\parallel}) = \tau_s(\omega, \mathbf{k}_{\parallel}) + \tau_p(\omega, \mathbf{k}_{\parallel})$, where the contributions of s- and p-polarized waves are given by [7]

$$\tau_{\alpha}(\omega, \mathbf{k}_{\parallel}) = \begin{cases} (1 - |r_{\alpha,21}|^2)(1 - |r_{\alpha,23}|^2)/|D_{\alpha}|^2, & k_{\parallel} < \omega/c \\ 4\text{Im}\{r_{\alpha,21}\}\text{Im}\{r_{\alpha,23}\}e^{-2|k_{\perp,2}|\Delta}/|D_{\alpha}|^2, & k_{\parallel} > \omega/c \end{cases} \quad (11)$$

Here, $\alpha = s, p$ and index 1 refers to the left plate, 2 to the vacuum gap, and 3 to the right plate. The coefficients $r_{\alpha,ij}$ are reflection or Fresnel coefficients of the two interfaces between gold and the vacuum gap and are given by

$$r_{s,ij} = \frac{k_{\perp,i} - k_{\perp,j}}{k_{\perp,i} + k_{\perp,j}} \quad \text{and} \quad r_{p,ij} = \frac{\epsilon_j k_{\perp,i} - \epsilon_i k_{\perp,j}}{\epsilon_j k_{\perp,i} + \epsilon_i k_{\perp,j}}, \quad (12)$$

where the component of the wavevector in system i perpendicular to the plates may also be expressed as $k_{\perp,i} = \sqrt{\epsilon_i \omega^2 / c^2 - k_{\parallel}^2}$ and $\epsilon_i(\omega)$ is the corresponding dielectric function. Finally, $D_{\alpha} = 1 - r_{\alpha,21} r_{\alpha,23} e^{2ik_{\perp,2}\Delta}$ is a Fabry-Pérot-like denominator, resulting from the multiple scattering between the two interfaces.

To compute the heat transfer coefficient, we have employed the experimental dielectric function for Au reported in Ref. 54. Our results basically coincide with

those reported in Ref. 55, with minor differences due to the different Au dielectric function employed here. We also find for small gaps in the near-field regime that the contribution of s-polarized evanescent waves, resulting from total internal reflection, completely dominates the radiative heat transfer all the way down to separations of about 1 Å. Let us remark that in the formalism detailed above, we make use of a local approximation, in which the dielectric function is assumed to depend only on frequency. However, non-local contributions due to the momentum dependence of the dielectric function have been shown to be negligible for gaps larger than 1 Å [55], as the ones studied in this work.

We can use the results for the heat transfer coefficient ζ to estimate the radiative thermal conductance in a junction with Au electrodes. For this purpose, we need to know the macroscopic shape of the electrodes. In STM-based experiments, the electrodes are a tip and planar surface. Thus, and since we are interested in the extreme near-field regime (with gaps in the order of nanometers), it is reasonable to model this situation with a finite sphere of a given radius R and an infinite planar surface. We shall refer to this geometry as tip-surface geometry. On the other hand, in the case of mechanically controllable break junctions, it is more appropriate to model the electrodes as two spherical tips. For simplicity we assume two spheres of the same radius R . We shall refer to this geometry as tip-tip geometry.

In principle, one can carry out a very accurate analysis of the radiative heat transfer in these two types of geometries along the lines of Ref. 11, but for our purposes here it suffices to make use of the so-called proximity approximation, sometimes referred to as Derjaguin approximation [56]. It has been shown to provide a very good approximation for the two geometries considered here in the limit in which the tip radius is much larger than the gap size [11, 41, 57, 58]. In particular, Kim *et al.* [11] showed that microscopic details like surface roughness (either at the tip or at the surface) do not significantly change the results for Au. Within the proximity approximation the radiative heat conductance between a sphere and a plane and between two spheres can be computed as

$$\kappa_{\text{pt}}(\Delta) = \int_0^R \zeta(h(r)) 2\pi r dr, \quad (13)$$

where Δ is the gap, ζ is the heat transfer coefficient calculated as described above, R is the sphere radius, and $h(r) = \Delta + R - \sqrt{R^2 - r^2}$ for the tip-surface geometry and $h(r) = \Delta + 2R - \sqrt{R^2 - r^2}$ for the tip-tip geometry, as depicted in Fig. 9(a).

Finally, let us point out that we do not take the presence of molecules into account in the calculation of the photonic thermal conductance. In the single-molecule junctions considered in this work, the molecules only modify the refractive index of the gap in a very tiny region. Due to the long-wavelength nature of the electromagnetic waves that dominate the NFRHT, this region

is orders of magnitude smaller than the portion of the electrodes that contribute to the radiative heat transfer [11]. Therefore, the role of the molecules in the photonic transport is expected to be negligible.

III. RESULTS

A. Charge transport, phonon transport and thermoelectric figure of merit

We start our discussion of the results by considering the geometries shown in Fig. 1(a) for an Au-C₆₀-Au and an Au-C₆₀-C₆₀-Au junction, which will be hereafter referred to as monomer and dimer junctions, respectively. In these particular geometries, the molecules make contact to three Au atoms of a blunt tip on the left, while they are bonded to a single Au atom of an atomically sharp tip at the right Au electrode. This asymmetric situation is meant to mimic the geometries realized in the STM experiments of Ref. 34, in which one of the electrodes is an Au surface and the other one an Au STM tip. Let us stress that these geometries were obtained by minimizing the total energy of the junctions as a function of the electrode separation d , yielding the distance d_0 . The distances d and d_0 are also visualized in Fig. 3(a). Using a coordinate system, oriented as depicted in Fig. 1, we find that the closest Au-C separation along the x -axis is roughly 1.8 Å from the blunt tip and 2.2 Å from the sharp tip. The x -axis separation between the two C₆₀ molecules in the dimer junction is approximately 3.0 Å. In Fig. 1(b)-(e) we summarize the thermoelectric transport properties for these two junctions by showing the electronic transmission as a function of energy, the corresponding phononic transmission, the thermopower as a function of temperature, and the electronic and phononic contributions to the heat conductance as a function of temperature.

For these blunt-sharp junctions, the electrical conductance is $0.23G_0$ for the monomer and $7.1 \times 10^{-4}G_0$ for the dimer. These values are close to the experimental values found in Ref. 34, where mean values of $0.1G_0$ and $1.8 \times 10^{-3}G_0$ were reported for the monomer and dimer junctions, respectively. Notice that in both cases the electronic transmission at the Fermi energy is determined by the LUMO of the molecules, as it has been reported in numerous studies, see for instance Ref. 31 and references therein.

With respect to the phononic transmission, one can see in Fig. 1(c) that the phonon conduction is dominated by low-lying vibrational modes with energies $E < 10$ meV. Let us recall that the Debye energy of the metal electrodes sets an upper limit for the energy of the vibrational modes that can contribute to the transport, which in our case is around 20 meV [38]. However, in the range between 10 and 20 meV there are no significant contributions to the phonon thermal conductance, which we attribute to the weak metal-molecule coupling for the

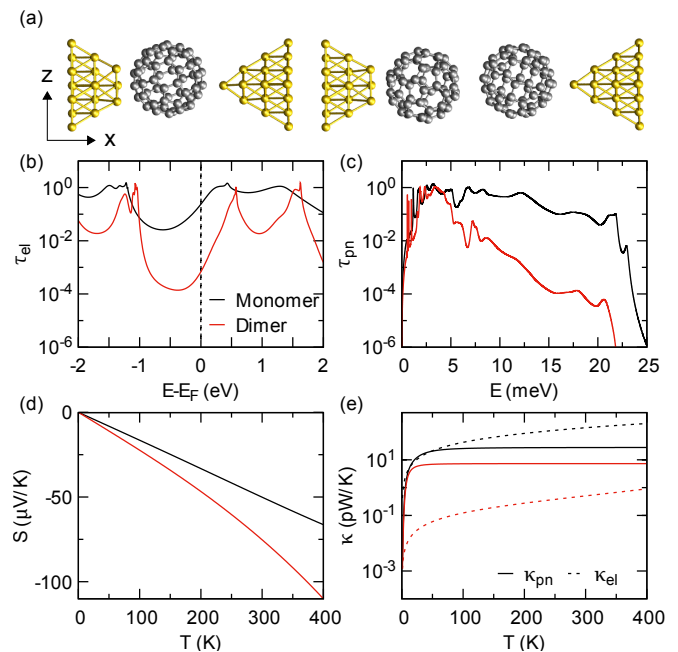


FIG. 1. (Color online) (a) Equilibrium geometries of C₆₀ monomer and C₆₀ dimer junctions. The molecules are bonded to blunt and sharp Au electrodes on the left and right. These geometries correspond to the minimum of the total energy with respect to the distance d between the electrodes. We call this particular separation for the equilibrium geometry d_0 , see illustration in Fig. 3(a). (b) Electronic transmission as a function of energy, measured with respect to the Fermi level, for the two geometries shown in panel (a). (c) Phonon transmissions as a function of energy. (d) Thermopower of the two junctions as a function of temperature. (e) Electronic and phononic contributions to the heat conductance as a function of temperature for both junctions. Data referring to the monomer is shown in black, those of the dimer in red.

modes in this energy range.

Turning now to the thermopower, we see in Fig. 1(d) that it approximately follows a linear dependence on temperature, as expected from the low-temperature expression in Eq. (7). In particular, the room-temperature thermopower has a value of -49.6μ V/K for the monomer and -75.3μ V/K for the dimer junction. The negative values are due to the fact that the electronic transport is dominated in both cases by the LUMO, meaning that electric conduction is electron-like. Notice also that the thermopower value for the dimer junction almost doubles that of the monomer, similar to what was observed in Ref. 34, while the absolute values are somewhat larger than those reported experimentally.

The temperature dependence of the different contributions to the heat conductance, displayed in Fig. 1(e), shows that both junctions behave qualitatively different, especially at room temperature. In the monomer junction the room-temperature electronic thermal conductance $\kappa_{el} = 142.0$ pW/K, which is very close to the

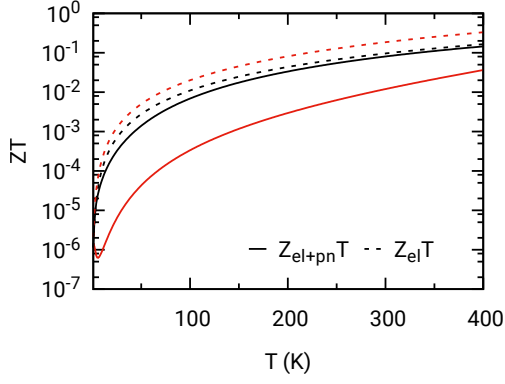


FIG. 2. (Color online) Figure of merit ZT as a function of temperature for the two geometries shown in Fig. 1(a). Black curves are for the monomer junction, while red ones are for the dimer. The solid lines correspond to $Z_{\text{el+pn}}T$, including both the electronic and phononic contributions to the heat conductance, $\kappa = \kappa_{\text{el}} + \kappa_{\text{pn}}$, while the dashed lines correspond to $Z_{\text{el}}T$, including only the electronic one, $\kappa = \kappa_{\text{el}}$.

value expected from the Wiedemann-Franz law, dominates over the phononic one, $\kappa_{\text{pn}} = 25.5$ pW/K. At the contrary, for the dimer junction the phononic contribution $\kappa_{\text{pn}} = 7.3$ pW/K dominates the thermal conductance and the electrons give an insignificant contribution of $\kappa_{\text{el}} = 0.5$ pW/K. Notice also that the total thermal conductance at room temperature is about 20 times larger for the monomer case than for the dimer case, which is mainly due to a dramatic decrease in the electronic contribution for the latter. For the sake of comparison, it is worth mentioning that we found in Ref. 39 that alkane-based chains of varying length exhibit phononic thermal conductance values ranging from 15 to 45 pW/K. Our results for these blunt-sharp C_{60} junctions show that there is a change in the dominant heat carriers as a function of the number of C_{60} molecules. This has a crucial impact on the figure of merit, as we proceed to discuss.

Results for the figure of merit ZT , see Eq. (1), are shown in Fig. 2. There we depict the evolution of $Z_{\text{el+pn}}T$ with temperature, taking into account both the electronic and phononic contributions to the thermal conductance, and $Z_{\text{el}}T$, taking into account only the electronic contribution. The first thing to notice is that at room temperature the monomer junction reaches a value of $Z_{\text{el}}T = 0.093$, which is only slightly reduced to $Z_{\text{el+pn}}T = 0.079$ by the phononic contribution to the thermal transport. However, in the dimer case the room-temperature value $Z_{\text{el}}T = 0.18$ is strongly reduced by the phonon heat conduction to $Z_{\text{el+pn}}T = 0.012$. Exploiting the Wiedemann-Franz law in Eq. (8), which we find to be well obeyed, we can write $ZT \approx S^2/[L_0(1 + \kappa_{\text{other}}/\kappa_{\text{el}})]$. With this relation the ZT values of the dimer junction can be interpreted as follows. Neglecting κ_{other} , the increase in $Z_{\text{el}}T$ for the dimer junction is due to the increase of the thermopower as compared with the monomer. Set-

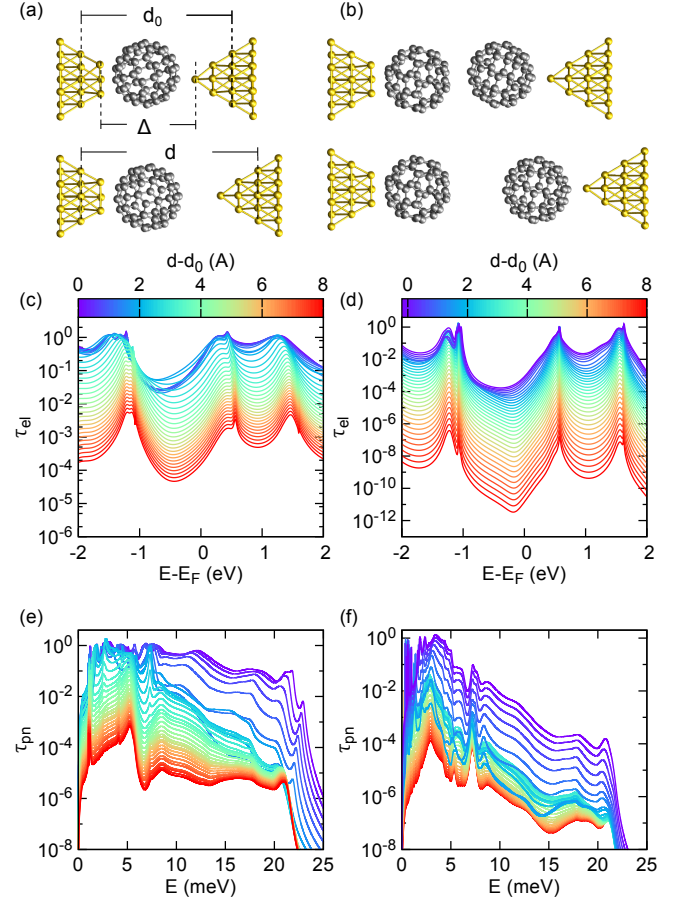


FIG. 3. (Color online) Evolution of the electronic and phononic transmissions with the elongation of the junctions in Fig. 1. (a) Geometries of the monomer junction. The upper geometry is the equilibrium geometry, already displayed in Fig. 1, while the lower junction is stretched. The distance d is measured between Au layers of the electrodes that are held fixed in the geometry optimization process, and d_0 is the separation for the equilibrium geometry. The gap distance Δ between the outer atoms of the Au electrodes that contact the molecules is somewhat shorter. (b) Same as in (a) but for the dimer junction. (c) Evolution of the electronic transmission of the monomer contact upon stretching as a function of the energy that is measured with respect to the Fermi energy. (d) The same as in panel (c) but for the dimer junction. (e) The corresponding evolution of the phononic transmission for the monomer junction. (f) The same as in panel (e) but for the dimer junction. We determine elongations as $d - d_0$, and plot the corresponding energy-dependent transmission curves in different colors as indicated by the color scale bar.

ting $\kappa_{\text{other}} = \kappa_{\text{pn}}$, we see from Fig. 1 that the phonon thermal conductance of the dimer is slightly lower than those of the monomer. But due to the much stronger decrease of the electrical conductance for two C_{60} as compared to a single one, leading to a corresponding reduction of κ_{el} via the Wiedemann-Franz law, the ratio

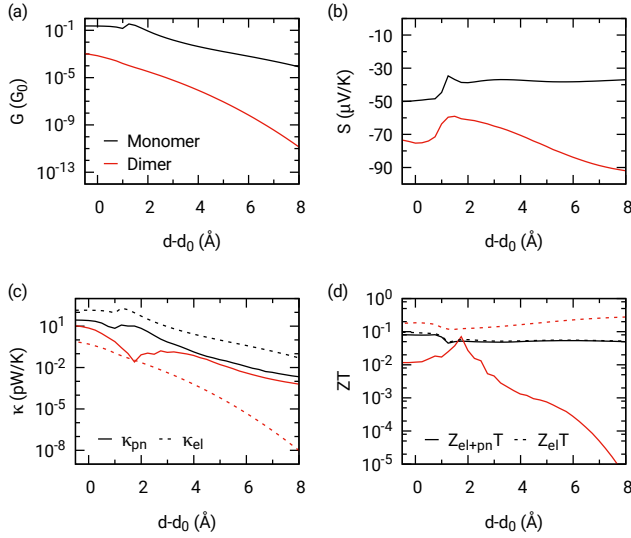


FIG. 4. (Color online) Transport coefficients at $T = 300$ K as a function of the distance $d - d_0$. The results are obtained from the transmission functions shown in Fig. 3. (a) Electrical conductance, (b) thermopower, (c) electronic and phononic thermal conductance, and (d) the corresponding figures of merit $Z_{\text{el+pn}}T$ and $Z_{\text{el}}T$. In all panels, black lines correspond to the monomer junction and red lines to the dimer junction.

$\kappa_{\text{pn}}/\kappa_{\text{el}}$ and the denominator $L_0(1 + \kappa_{\text{pn}}/\kappa_{\text{el}})$ get large, resulting in a pronounced suppression of $Z_{\text{el+pn}}T$ for the dimer. Thus, this first example of blunt-sharp monomer and dimer junctions indicates that because of the important contribution of phonon conduction to the thermal transport, the appealing suggestion of Ref. 34 that high ZT values may be achieved by stacking C_{60} molecules, as discussed in the introduction, is not backed up by our calculations.

To test the robustness of the main conclusions so far, especially the strong reduction of $Z_{\text{el+pn}}T$ as compared to $Z_{\text{el}}T$ for the dimer junction, we have studied the role of strain in the different transport properties. For this purpose, and in order to mimic the STM experiments of Ref. 34, we simulated the stretching and compression of the junctions shown in Fig. 1. The evolutions of the electronic and phononic transmissions for the monomer and dimer junctions are shown in Fig. 3. Here, the different curves correspond to different distances d between the electrodes, measured with respect to the distance in the equilibrium geometries d_0 , as defined in Fig. 3(a). The thermoelectric transport properties G , S , κ and ZT are shown in Fig. 4 as a function of $d - d_0$. As one can see in Fig. 4(a), the electrical conductance exhibits an exponential decay both for the monomer and the dimer, as expected, when the junctions break and enter the tunneling regime. At all distances, G is much lower for the dimer than for the monomer, as expected for off-resonant transport (see for instance the electronic transmissions in Fig. 3(c,d)). In this regime the thermopower remains

relatively constant, see Fig. 4(b), and for any distance the value for the dimer junction roughly doubles that of the monomer junction. With respect to the thermal conductance, both electronic and phononic contributions decay monotonically in the tunneling regime. And, like in the equilibrium geometry, we find that while for the monomer the electrons determine the thermal transport, in the dimer case the phonons dominate at almost all distances due to the largely reduced electronic thermal conductance of the dimer junctions. This fact is reflected in the behavior of $Z_{\text{el+pn}}T$ for both junctions, see Fig. 4(d), which is dictated by the electronic thermal conductance in the monomer case during the whole stretching process, while it is clearly limited by the phononic thermal conductance in the dimer junction. In other words, the main conclusion of the previous paragraph – that ZT values of dimer junctions are small due to phonon heat conduction – holds for the whole elongation process from the contact to the deep tunneling regime.

For completeness, let us now consider the role of the binding geometry. In particular, we now proceed to discuss the results for the equilibrium geometries shown in Fig. 5(a), where the molecules are bonded to both Au electrodes through atomically sharp tips. This kind of symmetric geometry is more likely to be realized in a break-junction configuration like that of Ref. 17. The results for the different transport properties G , S , κ_{el} and κ_{pn} are qualitatively similar to those of the blunt-sharp geometries discussed above. All the room temperature values of these properties are summarized in Table I together with the derived $Z_{\text{el}}T$ and $Z_{\text{el+pn}}T$ values. The main difference to the blunt-sharp geometries is the fact that the electronic transmission does not follow a Lorentzian-like shape around the Fermi energy, see Fig. 5(b). This peculiar energy dependence is the result of a quantum interference and its origin has been explained in detail in Ref. 32. This quantum interference leads to a rather steep transmission at the Fermi energy, which is in turn responsible for the particularly large values of the thermopower for these kind of binding geometries, see Fig. 5(d). The phononic thermal conductance in Fig. 5(e) is again determined by the transmission at energies below 10 meV, as visible in Fig. 5(c). Finally, κ_{el} in Fig. 5(e) is larger than κ_{pn} at $T = 300$ K for the monomer junction. This behavior is reversed for the dimer junction, where $\kappa_{\text{pn}} \gg \kappa_{\text{el}}$.

Thus, as in the case of the blunt-sharp geometries above, the room temperature thermal conductance is dominated by the electronic contribution in the monomer case, while phonon transport dictates the total value of the thermal conductance in the dimer case. This is reflected in the $Z_{\text{el}}T$ and $Z_{\text{el+pn}}T$ values of these junctions, see Fig. 6. For the monomer $Z_{\text{el}}T$ and $Z_{\text{el+pn}}T$ are very similar in the whole temperature range, while $Z_{\text{el+pn}}T$ is 1-3 orders of magnitude smaller than $Z_{\text{el}}T$. As it is clear from the data listed in Table I, at room temperature we find indeed $Z_{\text{el+pn}}T \approx Z_{\text{el}}T$ for the monomer, while for the dimer κ_{pn} reduces $Z_{\text{el+pn}}T$ as compared to $Z_{\text{el}}T$ by

TABLE I. Gap between the gold electrodes Δ and room temperature values of the different transport properties for the three types of monomer and dimer equilibrium geometries with $d = d_0$ of Figs. 1, 5, 7. The distances d, d_0, Δ are defined in Fig. 3.

junction type	Δ (nm)	G (G_0)	S ($\mu\text{V/K}$)	κ_{el} (pW/K)	κ_{ph} (pW/K)	$Z_{\text{el}}T$	$Z_{\text{el+pn}}T$
monomer, blunt-sharp tips	1.12	0.23	-49.6	142.0	25.5	0.093	0.079
dimer, blunt-sharp tips	2.12	7.1×10^{-4}	-75.3	0.5	7.3	0.185	0.012
monomer, sharp-sharp tips	1.18	0.11	-57.4	68.6	20.0	0.129	0.100
dimer, sharp-sharp tips	2.18	1.3×10^{-4}	-189.2	0.1	7.4	0.963	0.014
monomer, blunt-blunt tips	1.11	1.08	-41.9	572.7	46.3	0.077	0.071
dimer, blunt-blunt tips	1.91	2.3×10^{-3}	-96.9	1.8	7.0	0.273	0.057

more than one order of magnitude. This illustrates once more the key role played by phonon transport in these dimer junctions.

In Figs. 7 and 8 we show results for yet another binding geometry, where in this case the molecules are bonded to both electrodes through blunt tips, see Fig. 7(a). The room temperature values of the different thermoelectric transport properties are summarized in Table I. This binding geometry allows us to test our conclusions in a situation, where the metal-molecule coupling takes place

through several Au atoms on both sides. As one can see in these two figures, the main conclusions of our discussions above are confirmed again. In particular, $Z_{\text{el+pn}}T$ is very similar to $Z_{\text{el}}T$ for the monomer, since κ_{pn} is negligible as compared to κ_{el} , while there is a strong reduction of $Z_{\text{el+pn}}T$ as compared to $Z_{\text{el}}T$ for the dimer since κ_{pn} dominates over κ_{el} .

A major difference of the blunt-blunt geometry with respect to the previous two types of geometries is the fact that the stronger electronic metal-molecule coupling leads to a rather high electronic transmission at the Fermi energy, which is reflected both in the electrical conductance and in the electronic contribution to the thermal conductance. As it is clear from Table I, both G and κ_{el} increase monotonically for monomer and dimer junctions in the order of sharp-sharp, blunt-sharp, and blunt-blunt geometries. Let us emphasize that the metal-molecule binding geometry also limits the efficiency of phonon heat transfer in the monomer junctions, with the most efficient coupling for the blunt tips. Indeed we obtain a clear ordering of κ_{pn} , which increases from sharp-sharp to sharp-blunt and blunt-blunt junctions. However, the phonon thermal conductance of the dimer junctions is nearly insensitive to the metal-molecule coupling and limited by

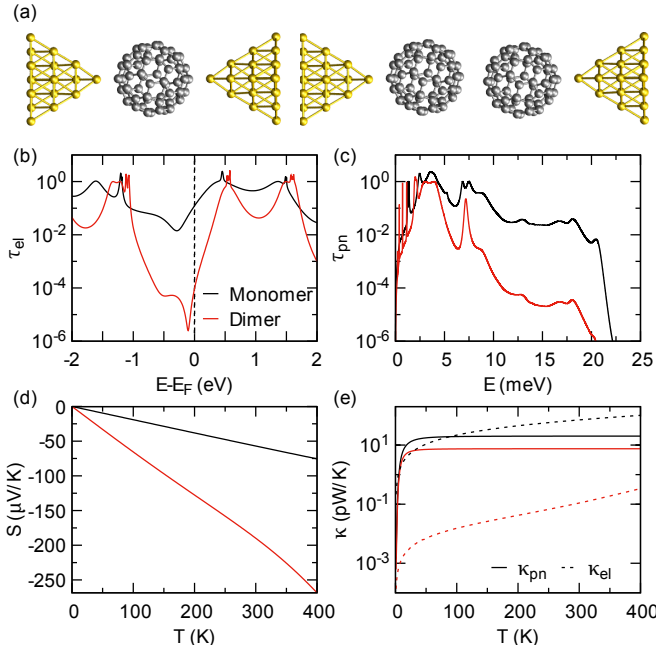


FIG. 5. (Color online) (a) Equilibrium geometries of a C_{60} monomer and a C_{60} dimer, bonded to both Au electrodes through atomically sharp tips. These geometries correspond to the minimum of the total energy with respect to the distance d between the electrodes, i.e. $d = d_0$. (b) Electronic transmission as a function of energy, measured with respect to the Fermi level, for the two geometries shown in panel (a). (c) Phonon transmissions as a function of energy. (d) Thermopower of the two junctions as a function of temperature. (e) Electronic and phononic contributions to the heat conductance for monomer and dimer junctions as a function of temperature. Data referring to the monomer is shown in black, those of the dimer in red.

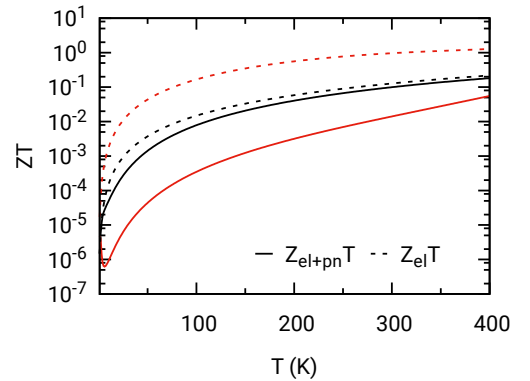


FIG. 6. (Color online) Figure of merit ZT as a function of temperature for the two geometries shown in Fig. 5(a). Black curves are for the monomer junction, while red ones are for the dimer. The solid lines correspond to $Z_{\text{el+pn}}T$, including both the electronic and phononic contributions to the heat conductance, $\kappa = \kappa_{\text{el}} + \kappa_{\text{pn}}$, while the dashed lines correspond to $Z_{\text{el}}T$, including only the electronic one, $\kappa = \kappa_{\text{el}}$.

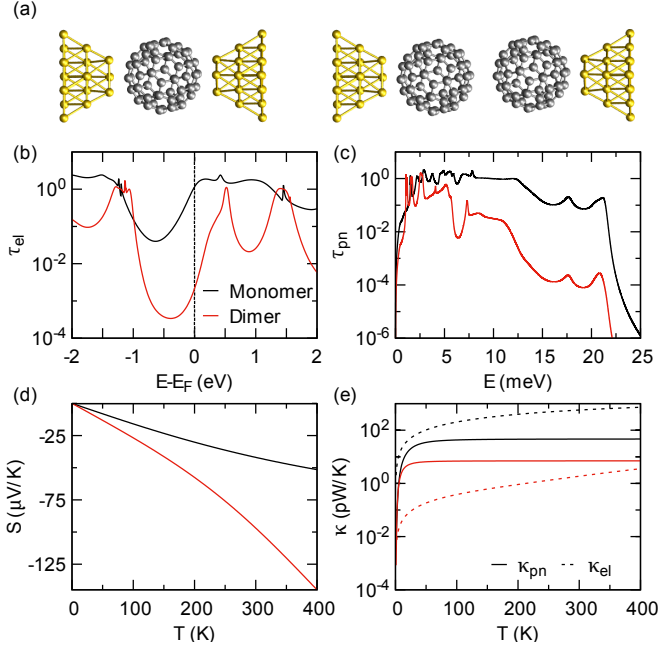


FIG. 7. (Color online) (a) Equilibrium geometries of a C₆₀ monomer and a C₆₀ dimer, bonded to both Au electrodes through blunt tips. These geometries correspond to the minimum of the total energy with respect to the distance d between the electrodes, i.e. $d = d_0$. (b) Electronic transmission as a function of energy, measured with respect to the Fermi level, for the two geometries shown in panel (a). (c) Phonon transmissions as a function of energy. (d) Thermopower of the two junctions as a function of temperature. (e) Electronic and phononic contributions to the heat conductance for monomer and dimer junctions as a function of temperature. Data referring to the monomer is shown in black, those of the dimer in red.

the weak molecule-molecule coupling.

Let us conclude this section by noting that we have also simulated the stretching of the sharp-sharp and blunt-blunt geometries (not shown here) and found that the main conclusions also apply there. In particular, we find in all of the cases that the phonon transport is very detrimental for the ZT values of the dimer junctions, while it plays a marginal role in the case of the monomer junctions.

B. Photon transport and thermoelectric figure of merit

The question that we want to address in this section is whether photon transport via thermal radiation can have an impact on the figure of merit of molecular junctions. Due to NFRHT the thermal conductance κ_{pt} can indeed largely exceed limits set by the Stefan-Boltzmann law for black bodies [7, 8]. We therefore put κ_{pt} in relation to κ_{el} and κ_{pn} , which were discussed before.

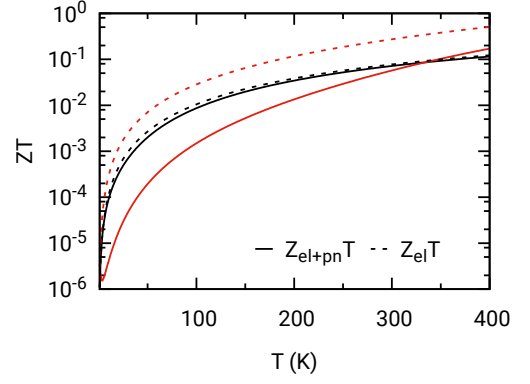


FIG. 8. (Color online) Figure of merit ZT as a function of temperature for the two geometries shown in Fig. 7(a). Black curves are for the monomer junction, while red ones are for the dimer. The solid lines correspond to $Z_{el+pn}T$, including both the electronic and phononic contributions to the heat conductance, $\kappa = \kappa_{el} + \kappa_{pn}$, while the dashed lines correspond to $Z_{el}T$, including only the electronic one, $\kappa = \kappa_{el}$.

As described in subsection IID, we use the formalism of fluctuational electrodynamics [53] to treat NFRHT. The results for the room temperature radiative heat conductance κ_{pt} , obtained with this procedure, are shown in Fig. 9 as a function of the gap size (or distance between the electrodes) Δ for the tip-surface and tip-tip geometries. We show these results in a relatively large gap-size range from 1 to 5 nm to provide an idea of the expectations for the photonic contribution to the thermal conductance in a wide range of molecular junctions. Notice that the radiative heat conductance changes quite slowly with the gap size.

For our purposes, we can assume that κ_{pt} basically remains constant in the range of studied electrode-to-electrode distances Δ . Defined as shown in Figs. 3 and 9 and listed in Table I, gap sizes Δ between the electrodes in our molecular junction geometries vary between 1 and 3 nm. Maximal elongations $d - d_0$, considered in Fig. 4, remain below 1 nm. The range of Δ , studied in Fig. 9, is thus compatible with the atomistic molecular junction models.

To relate κ_{pt} to κ_{el} and κ_{pn} , we consider again Table I. The comparison of the listed thermal conductances with Fig. 9 shows that, depending on the radius of the tip used to model the electrodes, the photonic contribution to the thermal conductance can be comparable or larger than the phononic one in the contact regime. In some cases κ_{pt} can even exceed the electronic contribution κ_{el} . This happens for both types of nanogap configurations, i.e. tip-surface and tip-tip geometries. It is obvious that κ_{pt} is particularly important in the tunneling regime. There it dominates the thermal transport, if junctions are stretched just by a few Å, see Fig. 4.

To illustrate the impact of κ_{pt} on the figure of merit, we display in Fig. 10 the ZT values as a function of the

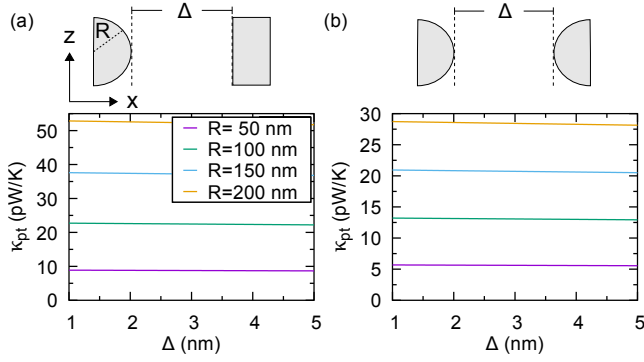


FIG. 9. (Color online) Room temperature radiative heat conductance as a function of the gap size for (a) a tip-surface geometry and (b) a tip-tip geometry. The different curves corresponds to different values of the radius of the spheres used to model the tips in both types of geometries.

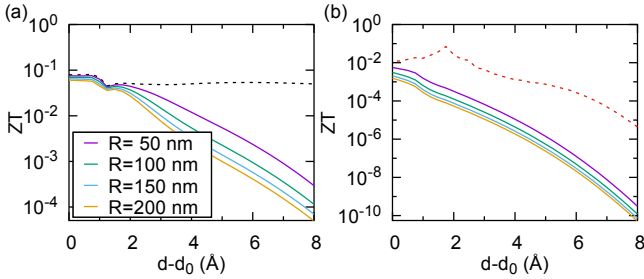


FIG. 10. (Color online) Comparison of the room temperature figure of merit $Z_{\text{el+pn+pt}}T$ (solid colored lines), including electronic, phononic and photonic contributions to the thermal conductance, with $Z_{\text{el+pn}}T$ (dashed lines), including only electronic and phononic parts, as a function of elongation for (a) the hollow-top monomer junction and (b) the hollow-top dimer junction. The dashed curves for $Z_{\text{el+pn}}T$ are identical to those shown in Fig. 4(d) and are reproduced to provide a reference. To determine the photonic heat conductance, the tip-surface geometry was assumed with tips of different radii R , as indicated by the legend.

displacement of the electrodes for the blunt-sharp junctions considered in Fig. 4. In particular, we show how the ZT values are modified by the photonic contribution for the tip-surface configuration and for various values of the tip radius. Notice that for elongations of the electrodes off the equilibrium by up to 2 Å, $Z_{\text{el+pn+pt}}T$ with $\kappa = \kappa_{\text{el}} + \kappa_{\text{pn}} + \kappa_{\text{pt}}$ for the monomer junction is similar to $Z_{\text{el+pn}}T$ that considers only electronic and phononic contributions. But for larger separations, $Z_{\text{el+pn+pt}}T$ breaks down dramatically. For the dimer junction, a suppression of $Z_{\text{el+pn+pt}}T$ as compared to $Z_{\text{el+pn}}T$ is obvious throughout the full range of elongations $d - d_0$ considered. Generally speaking, the detrimental influence of κ_{pt} on ZT is strongest in the tunneling regime for large

electrode separations.

IV. CONCLUSIONS

In summary, we have presented a systematic *ab initio* study of the role of the phonon transport in the thermal conductance and thermoelectric figure of merit of C_{60} -based molecular junctions. In particular, we have analyzed both monomer and dimer junctions, where the fullerenes are attached to gold electrodes. Taking only electrons and phonons into account, we have found that the thermal transport of monomer junctions is dominated by the electronic contribution irrespective of the binding geometry and elongation stage, while in the case of dimer junctions phonons dominate over electrons. This latter fact has important consequences for the thermoelectric figure of merit of dimer junctions, which is significantly reduced by the phononic thermal conductance. Our findings suggest that the proposal that stacks of C_{60} molecules could constitute a strategy to realize very efficient thermoelectric molecular devices is not justified.

On the other hand, we have also analyzed the importance of near-field thermal radiation for the figure of merit of molecular junctions. We have shown that, depending on the geometry of the molecular junction, the photonic contribution to the thermal conductance can be very significant and, in turn, detrimental for the performance of molecular junctions as thermoelectric devices. The photonic contribution is increasingly relevant in the tunneling regime, when covalent bonds to one of the electrodes are broken.

Overall our work sheds new light on the fundamental role of phonon and photon transport in the thermal conduction properties of molecular junctions. It shows the critical importance of understanding all factors determining the heat transport in order to assess the performance of these nanojunctions as potential energy conversion devices. We expect that our predictions can soon be verified experimentally by using techniques similar to those developed in Ref. 37.

V. ACKNOWLEDGMENTS

J.C.K. and F.P. gratefully acknowledge funding from the Carl Zeiss foundation and the Junior Professorship Program of the Ministry of Science, Research, and the Arts of the state of Baden Württemberg. J.C.C. was supported through the Spanish Ministry of Economy and Competitiveness (Contract No. FIS2014-53488-P) and thanks the German Research Foundation (DFG) and the Collaborative Research Center (SFB) 767 for sponsoring his stay at the University of Konstanz as Mercator Fellow. An important part of the numerical modeling was carried out on the computational resources of the bwHPC program, namely the bwUniCluster and the JUSTUS HPC facility.

-
- [1] J. C. Cuevas and E. Scheer, *Molecular Electronics: An Introduction to Theory and Experiment* (World Scientific, Singapore, 2010).
- [2] L. Cui, R. Miao, C. Jiang, E. Meyhofer, and P. Reddy, *J. Chem. Phys.* **146**, 092201 (2017).
- [3] L. Rincón-García, C. Evangeli, G. Rubio-Bollinger, and N. Agraït, *Chem. Soc. Rev.* **45**, 4285 (2016).
- [4] W. Lee, K. Kim, W. Jeong, L. A. Zotti, F. Pauly, J. C. Cuevas, and P. Reddy, *Nature* **498**, 209 (2013).
- [5] D. Segal and B. K. Agarwalla, *Annu. Rev. Phys. Chem.* **67**, 185 (2016).
- [6] H. J. Goldsmid, *Introduction to Thermoelectricity* (Springer, Berlin, 2016).
- [7] D. Polder and M. Van Hove, *Phys. Rev. B* **4**, 3303 (1971).
- [8] B. Song, A. Fiorino, E. Meyhofer, and P. Reddy, *AIP Advances* **5**, 053503 (2015).
- [9] A. Kittel, W. Müller-Hirsch, J. Parisi, S.-A. Biehs, D. Reddig, and M. Holthaus, *Phys. Rev. Lett.* **95**, 224301 (2005).
- [10] L. Worbes, D. Hellmann, and A. Kittel, *Phys. Rev. Lett.* **110**, 134302 (2013).
- [11] K. Kim, B. Song, V. Fernández-Hurtado, W. Lee, W. Jeong, L. Cui, D. Thompson, J. Feist, M. T. H. Reid, F. J. García-Vidal, J. C. Cuevas, E. Meyhofer, and P. Reddy, *Nature* **528**, 387 (2015).
- [12] K. Kloppstech, N. Könné, S.-A. Biehs, A. W. Rodriguez, L. Worbes, D. Hellmann, and A. Kittel, *Nat. Commun.* **8**, 14475 (2017).
- [13] L. Cui, W. Jeong, V. Fernández-Hurtado, J. Feist, F. J. García-Vidal, J. C. Cuevas, E. Meyhofer, and P. Reddy, *Nat. Commun.* **8**, 14479 (2017).
- [14] C. Joachim, J. K. Gimzewski, R. R. Schlittler, and C. Chavy, *Phys. Rev. Lett.* **74**, 2102 (1995).
- [15] H. Park, J. Park, A. K. L. Lim, E. H. Anderson, A. P. Alivisatos, and P. L. McEuen, *Nature* **407**, 57 (2000).
- [16] J. J. Parks, A. R. Champagne, G. R. Hutchison, S. Flores-Torres, H. D. Abruña, and D. C. Ralph, *Phys. Rev. Lett.* **99**, 026601 (2007).
- [17] T. Böhler, A. Edtbauer, and E. Scheer, *Phys. Rev. B* **76**, 125432 (2007).
- [18] N. Néel, J. Kröger, L. Limot, T. Frederiksen, M. Brandbyge, and R. Berndt, *Phys. Rev. Lett.* **98**, 065502 (2007).
- [19] M. Kiguchi, *Appl. Phys. Lett.* **95**, 073301 (2009).
- [20] G. Schull, T. Frederiksen, M. Brandbyge, and R. Berndt, *Phys. Rev. Lett.* **103**, 206803 (2009).
- [21] G. Schull, T. Frederiksen, A. Arnau, D. Sanchez-Portal, and R. Berndt, *Nat. Nanotech.* **6**, 23 (2011).
- [22] G. Schull, Y. J. Dappe, C. González, H. Bulou, and R. Berndt, *Nano Lett.* **11**, 3142 (2011).
- [23] J. J. Palacios, A. J. Pérez-Jiménez, E. Louis, and J. A. Vergés, *Phys. Rev. B* **64**, 115411 (2001).
- [24] J. J. Palacios, A. J. Pérez-Jiménez, E. Louis, and J. A. Vergés, *Nanotechnology* **12**, 160 (2001).
- [25] R. Stadler, S. Kubatkin, and T. Bjørnholm, *Nanotechnology* **18**, 165501 (2007).
- [26] T. Ono and K. Hirose, *Phys. Rev. Lett.* **98**, 026804 (2007).
- [27] M. K. Shukla, M. Dubey, and J. Leszczynski, *ACS Nano* **2**, 227 (2008).
- [28] X. Zheng, Z. Dai, and Z. Zeng, *J. Phys.: Condens. Matter* **21**, 145502 (2009).
- [29] E. Abad, C. González, J. Ortega, and F. Flores, *Org. Electron.* **11**, 332 (2010).
- [30] E. Abad, J. I. Martínez, J. Ortega, and F. Flores, *J. Phys.: Condens. Matter* **22**, 304007 (2010).
- [31] S. Bilan, L. A. Zotti, F. Pauly, and J. C. Cuevas, *Phys. Rev. B* **85**, 205403 (2012).
- [32] G. Géranton, C. Seiler, A. Bagrets, L. Venkataraman, and F. Evers, *J. Chem. Phys.* **139**, 234701 (2013).
- [33] S. K. Yee, J. A. Malen, A. Majumdar, and R. A. Segalman, *Nano Lett.* **11**, 4089 (2011).
- [34] C. Evangeli, K. Gillemot, E. Leary, M. T. González, G. Rubio-Bollinger, C. J. Lambert, and N. Agraït, *Nano Lett.* **13**, 2141 (2013).
- [35] S. K. Lee, T. Ohto, R. Yamada, and H. Tada, *Nano Lett.* **14**, 5276 (2014).
- [36] F. Pauly, J. K. Viljas, and J. C. Cuevas, *Phys. Rev. B* **78**, 035315 (2008).
- [37] L. Cui, W. Jeong, S. Hur, M. Matt, J. C. Klöckner, F. Pauly, P. Nielaba, J. C. Cuevas, E. Meyhofer, and P. Reddy, *Science* **355**, 1192 (2017).
- [38] M. Bürkle, T. J. Hellmuth, F. Pauly, and Y. Asai, *Phys. Rev. B* **91**, 165419 (2015).
- [39] J. C. Klöckner, M. Bürkle, J. C. Cuevas, and F. Pauly, *Phys. Rev. B* **94**, 205425 (2016).
- [40] F. Pauly, J. K. Viljas, U. Huniar, M. Häfner, S. Wohlthat, M. Bürkle, J. C. Cuevas, and G. Schön, *New J. Phys.* **10**, 125019 (2008).
- [41] B. Song, Y. Ganjeh, S. Sadat, D. Thompson, A. Fiorino, V. Fernández-Hurtado, J. Feist, F. J. García-Vidal, J. C. Cuevas, P. Reddy, and E. Meyhofer, *Nat. Nanotech.* **10**, 253 (2015).
- [42] TURBOMOLE GmbH Karlsruhe, TURBOMOLE, <http://www.turbomole.com>. TURBOMOLE was a development of the University of Karlsruhe and Forschungszentrum Karlsruhe from 1989 to 2007, and development has been undertaken by TURBOMOLE GmbH since 2007.
- [43] P. Deglmann, F. Furche, and R. Ahlrichs, *Chem. Phys. Lett.* **362**, 511 (2002).
- [44] P. Deglmann, K. May, F. Furche, and R. Ahlrichs, *Chem. Phys. Lett.* **384**, 103 (2004).
- [45] J. P. Perdew and Y. Wang, *Phys. Rev. B* **45**, 13244 (1992).
- [46] J. P. Perdew, K. Burke, and M. Ernzerhof, *Phys. Rev. Lett.* **77**, 3865 (1996).
- [47] S. Grimme, J. Antony, S. Ehrlich, and H. Krieg, *J. Chem. Phys.* **132**, 154104 (2010).
- [48] F. Weigend and R. Ahlrichs, *Phys. Chem. Chem. Phys.* **7**, 3297 (2005).
- [49] F. Weigend, *Phys. Chem. Chem. Phys.* **8**, 1057 (2006).
- [50] U. Sivan and Y. Imry, *Phys. Rev. B* **33**, 551 (1986).
- [51] L. G. C. Rego and G. Kirczenow, *Phys. Rev. Lett.* **81**, 232 (1998).
- [52] N. Mingo and L. Yang, *Phys. Rev. B* **68**, 245406 (2003).
- [53] S. M. Rytov, Y. A. Kravtsov, and V. I. Tatarskii, *Principles of Statistical Radiophysics 3: Elements of Random Fields* (Springer, Berlin, 1989).
- [54] M. A. Ordal, L. L. Long, R. J. Bell, S. E. Bell, R. R. Bell, R. W. Alexander, and C. A. Ward, *Appl. Opt.* **22**, 1099 (1983).

- [55] P.-O. Chapuis, S. Volz, C. Henkel, K. Joulain, and J.-J. Greffet, Phys. Rev. B **77**, 035431 (2008).
- [56] B. V. Derjaguin, I. I. Abrikosova, and E. M. Lifshitz, Q. Rev. Chem. Soc. **10**, 295 (1956).
- [57] K. Sasihithlu and A. Narayanaswamy, Phys. Rev. B **83**, 161406 (2011).
- [58] C. Otey and S. Fan, Phys. Rev. B **84**, 245431 (2011).